Self-assembling TiO2 nanorods on large graphene oxide sheets at a two-phase interface and their anti-recombination in photocatalytic applications

Liu, Jincheng; Bai, Hongwei; Wang, Yinjie; Liu, Zhaoyang; Zhang, Xiwang; Sun, Darren Delai

2010

Liu, J., Bai, H., Wang, Y., Liu, Z., Zhang, X., & Sun, D. D. (2010). Self-assembling TiO2 nanorods on large graphene oxide sheets at a two-phase interface and its anti-recombination in photocatalytic application. Advanced Functional Materials, 20, 4175-4181.

https://hdl.handle.net/10356/92143

https://doi.org/10.1002/adfm.201001391

Self-Assembling TiO_2 Nanorods on Large Graphene Oxide Sheets at a Two-Phase Interface and Their Anti-Recombination in Photocatalytic Applications

By *Jincheng Liu,* Hongwei Bai, Yinjie Wang, Zhaoyang Liu, Xiwang Zhang,* and *Darren Delai Sun**

TiO_2 nanorods are self-assembled on the graphene oxide (GO) sheets at the water/toluene interface. The self-assembled GO–TiO_2 nanorod composites (GO–TiO_2 NRCs) can be dispersed in water. The effective anchoring of TiO_2 nanorods on the whole GO sheets is confirmed by transmission electron microscopy (TEM), X-ray diffraction (XRD), Fourier transform IR spectroscopy (FTIR), and thermogravimetric analysis (TGA). The significant increase of photocatalytic activity is confirmed by the degradation of methylene blue (MB) under UV light irridiation. The large enhancement of photocatalytic activity is caused by the effective charge anti-recombination and the effective absorption of MB on GO. The effective charge transfer from TiO_2 to GO sheets is confirmed by the significant photoluminescence quenching of TiO_2 nanorods, which can effectively prevent the charge recombination during photocatalytic process. The effective absorption of MB on GO is confirmed by the UV-vis spectra. The degradation rate of MB in the second cycle is faster than that in the first cycle because of the reduction of GO under UV light irradiation.

1. Introduction

Developing high efficiency and stable photocatalytic materials for the elimination of global air and water pollution has attracted increasing amount of attention during the past decades. TiO_2 is the most studied photocatalytic material due to its chemical stability, non-toxicity and high photocatalytic activity in the removal of pollutants in water and air.[1] During the photocatalytic process, the electrons are excited from the valence band (VB) of TiO_2 to the conduction band (CB).[2,3] Hence, the effective electron-hole pairs are generated.[2,3] However, excited-state conduction-band electrons and valence-band holes can be recombined and dissipated as heat easily within a few seconds before they arrive at the photocatalyst surface,[4] which results in the loss in the efficiency of photocatalytic activity. Many methods of preventing the electron-hole recombination have been reported, such as using TiO_2 composites with noble metals,[5–7] metal oxides,[8–10] and carbon nanotubes (CNT).[11–14] Compared with noble metals and metal oxides, functionalized CNT can be effectively chemically bonded to TiO_2, which provides more effective charge transfer from TiO_2 to CNT to prevent the charge recombination for gaining higher efficiency of photocatalytic activity.

In comparison with CNT, graphene has perfect sp^2-hybridized two-dimensional carbon structure with better conductivity and larger surface area as unrolled CNT.[15,16] Furthermore, graphene is easy to produce from natural graphite through chemical oxidation-dispersion-reduction procedure at a low cost.[17] Through chemical oxidation, natural graphite can be effectively oxidized and exfoliated into graphene oxide (GO) with the introduction of oxygen-containing functional groups.[17] The presence of oxygen-containing functional groups in GO and reduced graphene makes them as excellent supporters to anchor inorganic nanocrystals for enhancement of wide applications.[18–21]

To date, there are only a few reports in the synthesis and application of graphene–TiO_2 nanocrystalline composites.[22–25] Williams et al. produced GO–TiO_2 nanocrystalline composites by sonicating the dispersed TiO_2 nanoparticles and GO in ethanol[22] and found the photocatalytic reduction of GO by TiO_2 under UV light irridiation. Wang et al. and Lambert et al. reported the synthesis of graphene–TiO_2 nanocrystalline composites by a one-step hydrothermal process.[23,24] Zhang et al. produced graphene–P25 TiO_2 composites through hydrothermal reaction and investigated its application in photocatalytic degradation of methylene blue.[25] However in their work, only several P25 nanoparticles were anchored to the graphene sheets on the edge. As we know, the one-dimensional TiO_2 nanocrystals with small size have large surface area and high quantum size effect, which makes it an ideal candidate for the photocatalytic and optoelectronic applications.[26,27] Hence, it is important to create these self-assembling TiO_2 nanorods with small size on the whole large GO sheets to achieve high efficiency photocatalytic application.

[*] Dr. J. Liu, H. Bai, Y. Wang, Z. Liu, X. Zhang, Prof. D. D. Sun
School of Civil and Environmental Engineering
Nanyang Technological University
Singapore, 639798
E-mail: JCLIU@ntu.edu.sg; DDSun@ntu.edu.sg

DOI: 10.1002/adfm.201001391

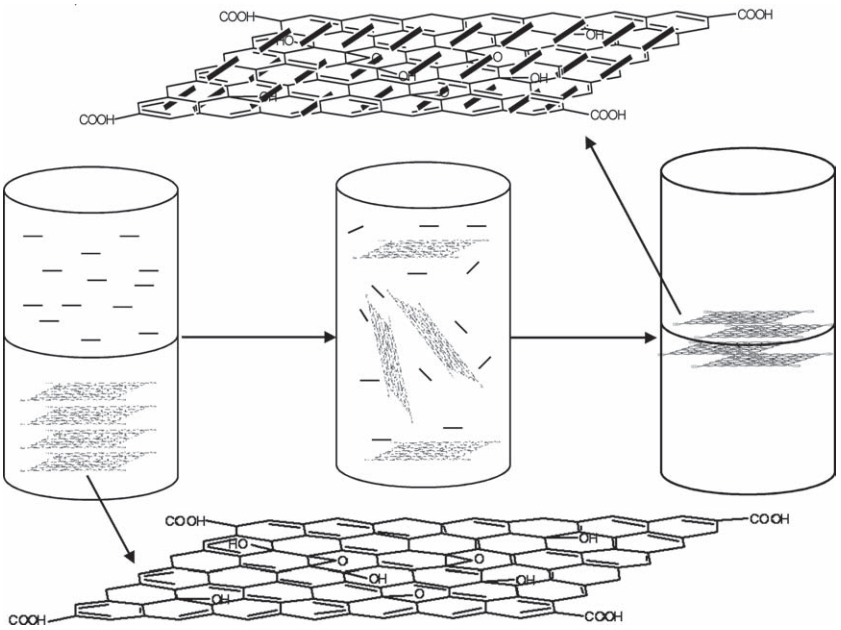

Scheme 1. Schematic presentation of self-assembly at the two-phase interface.

In this work, we assembled TiO_2 nanorods on large GO sheets at a water/toluene interface to produce GO–TiO_2 nanorod composites (GO–TiO_2 NRCs) for high efficiency photocatalytic application. TiO_2 nanorods stabilized by oleic acid (OLA–TiO_2) were synthesized by a low-temperature hydrolysis approach in advance.[28] The GO sheets oxidized by Hummers' method were exfoliated and dispersed in DI water.[29] The toluene solution of OLA–TiO_2 and the aqueous solution of GO were then mixed and stirred for 24 h. The self-assembly of TiO_2 nanorods on the large GO sheets occurs in the water/toluene interface (**Scheme 1**). The large GO sheets act as excellent supporters and stabilizers for the TiO_2 nanorods. The charge transfer from TiO_2 to GO and the adsorption of methylene blue (MB) by GO were investigated. The photocatalytic application for the degradation of MB was examined. To our knowledge, it is the first time that the graphene–TiO_2 nanocrystal composites are produced through a two-phase approach. The two-phase self-assembling procedure is facile and reproducible, and it can also be widely used for self-assembling other nonpolar organic soluble nanocrystals on large GO sheets easily.

2. Results and Discussion

2.1. Characterization of GO–TiO_2 NRCs

The as-prepared anatase TiO_2 nanorods of 2–4 nm diameter and 20–30 nm length (**Figure 1a**) were dispersed in toluene for further self-assembly process. The GO sheets was dispersed in deionized (DI) water with the size of 1 μm (Figure 1b). As shown in Figure S1.1 (Supporting Information), GO and TiO_2 nanorods were dispersed in water and toluene separately at the start. After stirring for 24 h, GO and TiO_2 nanorods were combined together at the water/toluene interface.

The morphology of GO–TiO_2 NRCs shown in Figure 1c–f. In Figure 1c, the single layer and double layer GO sheets are entirely covered by TiO_2 nanorods. Figure 1d shows a single sheet of GO–TiO_2 NRCs. It can be observed that TiO_2 nanorods exist homogeneously in the whole GO single sheet without obvious aggregation. Both the edge of graphene and the nanostructure of the TiO_2 nanorods are clearly observable in the higher magnification image of Figure 1e. Figure 1f gives the high-resolution transmission electron microscopy (HRTEM) images of GO–TiO_2 NRCs. The clear lattice of TiO_2 nanorods indicates that the TiO_2 nanorods are of high crystallinity. The transmission electron microscopy (TEM) analysis confirms the successful self-assembling TiO_2 nanorods on the whole large GO sheets. After adding the strong base, NaOH, into the aqueous solution of GO–TiO_2 NRCs, TiO_2 nanorods can be detached with the GO sheets (Figure S1.2, Supporting Information).

Figure 2a shows the X-ray powder diffraction (XRD) patterns of the starting graphite (natural graphite flake), GO obtained by Hummers' method, GO–TiO_2 NRCs, and OLA–TiO_2. The diffraction pattern of GO has a peak centered at $2\theta = 11.9°$, corresponding to the [001] interlayer spacing of 7.43 Å.[30] The XRD pattern of GO–TiO_2 NRCs shows clearly diffraction peaks of anisotropic anatase TiO_2,[31] which are without any change in comparison with OLA–TiO_2. However, the [001] reflections

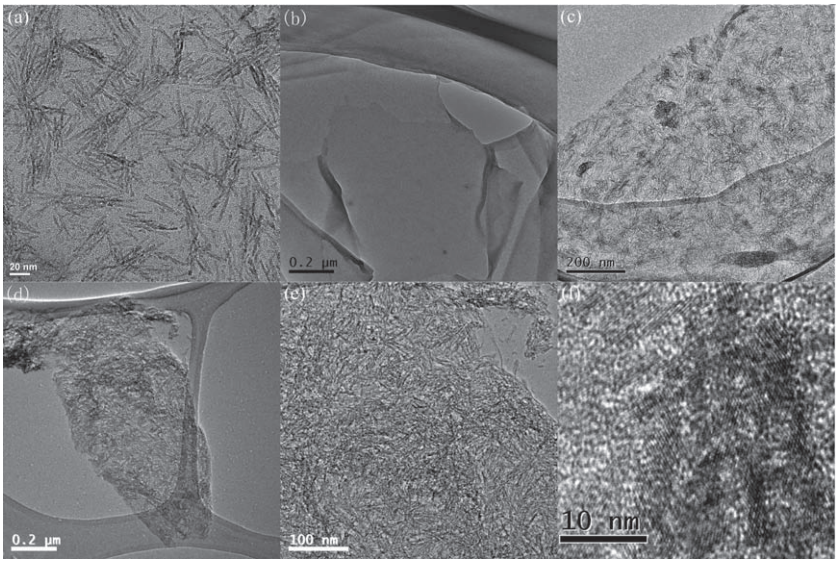

Figure 1. TEM images of TiO_2 nanorods, GO, and GO–TiO_2 NRCs.

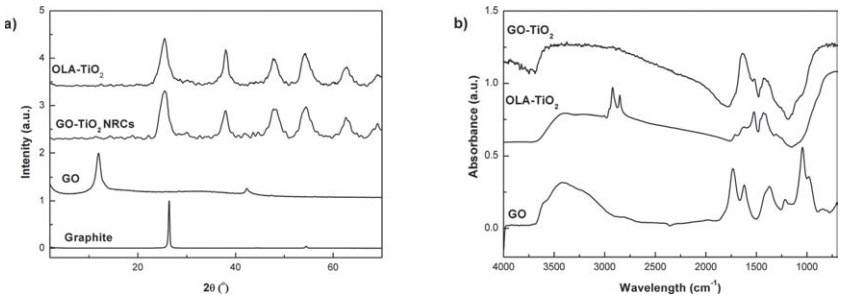

Figure 2. a) XRD patterns of OLA–TiO_2, GO–TiO_2 NRCs, GO, and graphite. b) FTIR absorption spectra of GO–TiO_2 NRCs, OLA–TiO_2, and GO.

of GO are not observed in the XRD pattern of GO–TiO_2 NRC sample because the regular stack of GO was destroyed by the intercalation of TiO_2 nanorods.[30,32] The XRD analysis further confirms that TiO_2 nanorods have been effectively intercalated into the GO stacks.

Figure 2b shows the Fourier transform infrared (FTIR) spectra of GO, GO–TiO_2 NRCs, and OLA–TiO_2. As shown in Figure 2b, the FTIR spectrum of GO reveals that the C=O and C–O stretching vibration bands of COOH groups are at 1730 and 1039 cm^{-1}.[33] This indicates that the graphite was sufficiently oxidized into hydrophilic GO with hydroxyl and carboxyl groups. For the FTIR of OLA–TiO_2 and GO–TiO_2 NRCs, the broad bands from approximately 950 to 800 cm^{-1} results from the characteristic vibrations of the inorganic Ti–O–Ti network.[34] The FTIR spectrum of OLA–TiO_2 shows the doublet bands at 2854 and 2923 cm^{-1}, which are attributed to the antisymmetric and symmetric C–H stretching vibrations from oleic acid.[35] The doublet bands (at 1525 and 1432 cm^{-1}) are assigned to the COO^- antisymmetric and symmetric stretching vibrations complexed with surface Ti centers.[36] After combined with GO, the FTIR spectrum of GO–TiO_2 NRCs shows doublet bands of the COO^- antisymmetric and symmetric stretching vibrations at 1521 and 1426 cm^{-1}, respectively. Moreover, the lack of the C–H stretching vibrations at 2854 and 2923 cm^{-1} indicates that the oleic acid ligands are completely removed. The complete clearance of oleic acid will further expand the application of TiO_2 nanorods. Gutiérrez-Tauste et al. reported the bidentate coordination between the phenolic hydroxyl groups of dopamine and TiO_2.[37] Similar to the dopamine molecular, GO has large quantity of phenolic hydroxyl groups, which can coordinate with TiO_2 nanorods. Although most carboxyl groups are on the edge of GO,[38] TiO_2 nanorods are located in the whole GO sheets because of the coordination between phenolic hydroxyls and TiO_2, which is in accordance with our TEM observations.

Thermogravimetric analysis (TGA) is an effective analytical technique to evaluate the ratio of GO/TiO_2. From **Figure 3**, the TGA curve of GO–TiO_2 NRCs shows 12% weight loss from 30 to 100 °C, which is due to the loss of water or some organic solvent molecular. The mass loss from 200 to 530 °C is 26% and belongs to the decomposition of oxygen group and carbon oxidation from GO.[38] Compared with GO, which shows the complete decomposed temperature of carbon at 710 °C, GO–TiO_2 NRCs shows a significant lower temperature at 530 °C, to fully decompose the carbon of GO. This suggests that the thermal stability of GO is decreased after composited with TiO_2 nanorods due to the catalysis effect of TiO_2. The 62% residue is associated with the TiO_2 nanorods. According to the TGA analysis (Figure 3), the mass ratio of GO:TiO_2 nanorods is 0.45.

The TEM, XRD, FTIR, and TGA analyses confirm the effective self-assembly of TiO_2 nanorods at large GO sheets at the water/toluene interface. The reason for the effective self-assembly by the two-phase method is that TiO_2 nanorods immediately leave the organic phase after adhering to GO sheets. The prerequisite of successful self-assembly is the good dispersion of both TiO_2 and GO. For comparison, GO (45 mg) and Degussa P25 (100 mg) are used to fabricate GO–P25 composites. Because P25 is not dispersed in deionized (DI) water very well, only some of the P25 nanoparticles are anchored to the GO sheets (Figure S1.3, Supporting Information). Moreover, in the two-phase self-assembly process it is easy to control the GO/TiO_2 ratio by decreasing the TiO_2 quantity.

2.2. Photocatalytic Application of GO–TiO_2 NRCs in the Degradation of MB

The photocatalytic activity of GO–TiO_2 NRCs is evaluated by the degradation of MB (10 ppm) under UV light irradiation (λ = 254 nm, 11 W, and the light intensity of 5.4 mW cm^{-2}). The photocatalytic degradation of MB is monitored by the UV-vis absorption spectra of MB in aqueous solutions. The real-time concentration of MB during photocatalytic degradation is proportional to the normalized maximum absorbance. As shown in **Figure 4a**, MB in water shows a strong absorption band centered at 602 nm, which is assigned to the dimer of MB.[39] After photocatalytic degradation with P25 and OLA–TiO_2, the relative intensities of absorption band at 602 nm significantly decrease to 32% and 30%, respectively. The absorption bands of MB dimer at 602 nm has disappeared after photocatalytic degradation by GO–TiO_2 NRCs and GO–P25 composites under UV

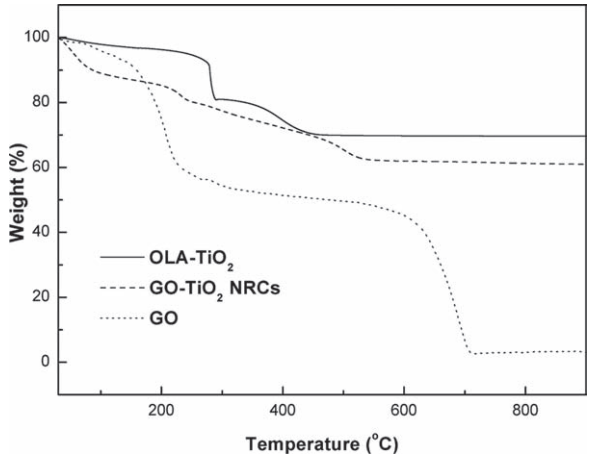

Figure 3. TGA curves of OLA–TiO_2, GO–TiO_2 NRCs, and GO.

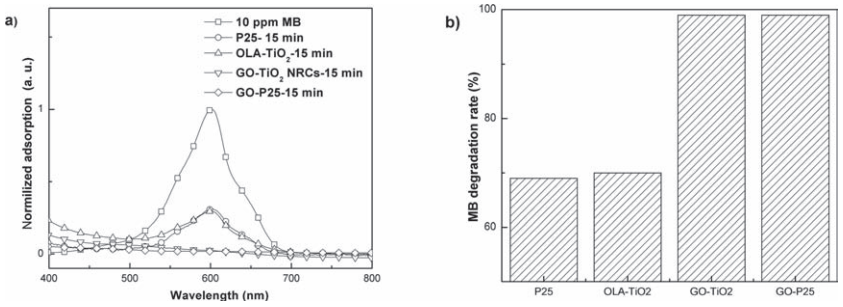

Figure 4. a) UV-vis absorption of MB and MB after photocatalytic degradation by P25, OLA–TiO_2, GO–TiO_2 NRCs, and GO–P25 composites under UV light (λ = 254 nm) for 15 min. b) MB degradation rate (%) under UV light (λ = 254 nm) for 15 min.

light irradiation for 15 min. Detailed MB degradation rate by P25, OLA–TiO_2, GO–TiO_2 NRCs, and GO–P25 composites are given by Figure 4b. It can be seen that the photocatalytic activity on MB degradation significantly increases after self-assembling TiO_2 nanorods or P25 on GO sheets.

The adsorption of contaminant molecule is helpful for the increase of photocatalytic activity. The UV-vis absorption spectra were tested for investigating the adsorption and desorption of MB on GO. As shown in **Figure 5a**, the disappearance of the absorption bands of MB at 602 nm suggests that MB is well-absorbed by GO sheets. Because of similar conjugated aromatic cycles, the interaction of π-conjugated and the ion-dipole interactions between GO and MB will take place, which leads to the adsorption of MB by GO sheets. However, the interaction of π-conjugated and the ion-dipole interactions can be destroyed by adding the strong base, NaOH. As shown from Figure 5a, the absorption band centered at 500 nm can be observed, which is assigned to the absorption of MB in the basic circumstance.[40] After being neutralized by HCl, the absorption of MB shows the strong peaks centered at 602 nm with the same intensity as that of the original MB solution. This indicates that MB molecule can be effectively adsorbed by GO sheets without degradation. The effective adsorption is helpful to enhance the photocatalytic activity in the degradation of MB.

The absorption of the bonding GO–TiO_2 NRCs plays an important role in the photocatalytic activity. As shown by Figure 5b, the OLA–TiO_2 shows the absorption onset at 325 nm, which indicates a strong quantum size effect in TiO_2 nanorods of small diameter. After combined with GO, the absorption onset of GO–TiO_2 NRCs has a significant red shift to 400 nm, which is caused by the bonding effect between GO and TiO_2. Similar results were reported by Williams et al. and Zhang et al.[22,25] However, the absorption onset of GO–P25 composites shows only a weak quantization of red shifts compared with P25 due to fewer P25 nanoparticles anchored to the GO sheets. The extended absorption is important for the photocatalytic application of GO–TiO_2 NRCs under visible light.

The efficient charge separation and transfer are crucial for the enhanced photocatalytic activity of GO–TiO_2 NRCs. The photoluminescence (PL) spectra of OLA–TiO_2, GO–TiO_2 NRCs, P25, and GO–P25 composites excited at 280 nm are given in Figure 5c (The OLA–TiO_2 and GO–TiO_2 NRCs are dispersed in tetrahydrofuran (THF) solution while the P25 and GO–P25 composites are dispersed in DI water, $[TiO_2]$ = 0.5 mol L^{-1}).

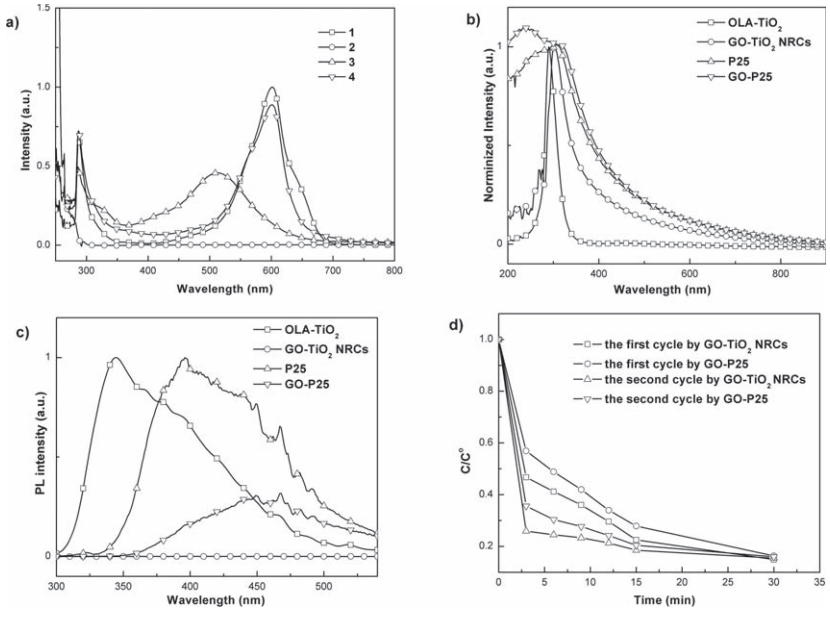

Figure 5. a) UV-vis absorption of 1) original MB solutions (10 ppm), 2) centrifuged upper clear solution of MB (10 ppm) and GO mixture (0.5 mg mL^{-1}), 3) the centrifuged upper clear solution from MB (10 ppm), GO (0.5 mg mL^{-1}) and NaOH (0.5 mg mL^{-1}), and 4) the solution (3) neutralized by 2 drops of 36.5% HCl, b) UV-vis absorption spectra of OLA–TiO_2, GO–TiO_2 NRCs, P25, and GO–P25 composites. c) PL spectra of OLA–TiO_2, GO–TiO_2 NRCs, P25, and GO–P25 composites. OLA–TiO_2 and GO–TiO_2 NRCs were dispersed in THF for UV-vis absorption and PL testing while P25 and GO–P25 composites were dispersed in DI water for UV-vis absorption and PL tests. d) Cyclic photocatalytic degradation experiments of MB (50 ppm) by GO–TiO_2 NRCs and GO–P25 composites under UV light irridiation (λ = 254 nm).

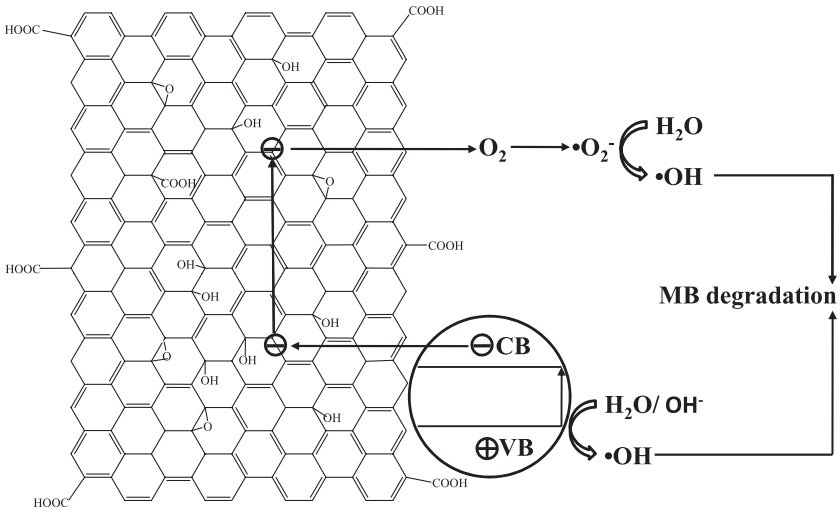

Scheme 2. The mechanical illustration of high photocatalytic activity for GO–TiO_2 NRCs.

The OLA–TiO_2 shows a strong PL emission band at 345 nm, which is assigned to the direct transition from X1b to X2b.[41] After combined with GO, the PL spectrum of GO–TiO_2 NRCs is completely quenched, which is caused by the electron transfer from the CB of TiO_2 to GO. However, the percentage of PL quenching for GO–P25 is only 70%. This is because only part of P25 nanoparticles are anchored with the GO sheets. According to the modified mechanism proposed by Hoffmann et al.,[42] the remaining hole in TiO_2 nanorods can take part in the redox reactions in the photocatalytic process. Yu et al. and Kuo reported the electron in the CNT could react with absorbed O_2 to form •OH.[11,43] Since GO has the similar structure to CNT, we speculate that the electron can transport along the GO sheets and then react with the absorbed O_2 to form •OH for the further photocatalytic degradation of MB. The schematic illustration of the charge transfer and enhanced photocatalytic activity by GO–TiO_2 NRCs is summarized in **Scheme 2**. The effective charge transfer can reduce the charge recombination and increase the photocatalytic activity of TiO_2 nanorods.

For investigating the long-term stability of GO–TiO_2 NRCs under UV light irradiation, the photocatalytic activities of GO–TiO_2 NRCs (73 mg) on the degradation of MB (50 ppm) under UV light irradiation during the photocatalytic degradation cycles were tested. For comparison, the photocatalytic degradation of MB by GO–P25 (73 mg) with the same GO/TiO2 ratio was studied. As shown in Figure 5d, the photocatalytic reactions apparently obeyed first-order kinetics and the photocatalytic reaction can be simply described by $dC/dt = kC$, where C is the concentration of MB and k denotes the overall degradation rate constant. The k (min^{-1}) constants for GO–TiO_2 NRCs at first cycle, GO–P25 composites at the first cycle, GO–TiO_2 NRCs at second cycle and GO–P25 composites at the second cycle are 0.263, 0.197, 0.855, and 0.630, respectively. It is apparent that the photocatalytic degradation rates of MB by GO–TiO2 NRCs are faster than that by GO–P25 composites during two cycles, which is due to the better contact between GO and TiO2 nanorods and the more effective charge transfer from TiO2 nanorods to GO sheets. It also can be seen that the photocatalytic degradation rates of MB during the second cycle are faster than that of the first cycle for both GO–TiO2 NRCs and GO–P25 composites. During the photocatalytic process, the GO sheets can be reduced by TiO_2 under UV light irradiation.[22] As shown from the X-ray photoelectron spectroscopy (XPS) spectra in **Figure 6**, the respective O:C atomic ratios for GO, GO–TiO_2 NRCs, and GO–TiO_2 NRCs after the photocatalytic degradation of MB are 0.236, 0.213, and 0.164. It is clear that the photocatalytic application of GO–TiO_2 NRCs under UV light resulted in an evident decrease in oxygen content, which will further enhance the conductivity of GO sheets. According to the mechanism by Hoffman et al.[41] the higher conductivity leads to more effective charge separation and more effective antirecombination during photocatalytic process. Consequently, the photocatalytic activity of GO–TiO2 NRCs will be improved after the first photocatalytic cycle. The GO–TiO_2 NRCs with high photocatalytic activity are promising for further applications in water treatment and dye-sensitized solar cells.

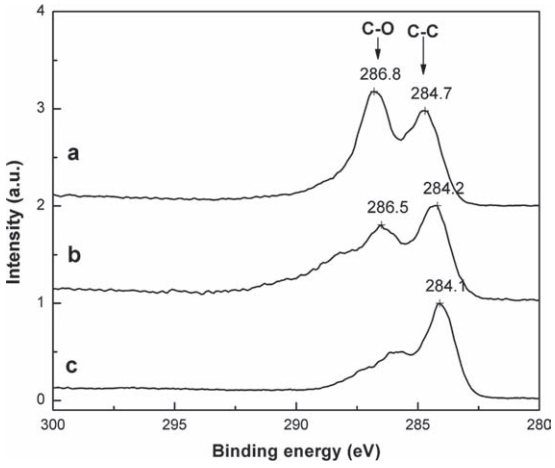

Figure 6. High-resolution XPS spectra in the C1s region a) GO, b) GO–TiO_2 NRCs, and c) the DI water washed photocatalyzed mixture of GO–TiO_2 NRCs (73 mg) and MB (5 mL, 0.010 mg mL^{-1}) under UV light irradiation ($\lambda = 254$ nm) for 15 min.

3. Conclusions

In summary, we have developed a water/toluene two-phase process for self-assembling TiO_2 nanorods on the whole large GO sheets. The GO–TiO_2 NRCs have much higher photocatalytic activity than GO–P25 and the original TiO_2 nanorods. We also demonstrated the effective absorption of contaminant MB by large GO sheets and the effective charge transfer from TiO_2 nanorods to large GO sheets, which is the mechanism of anti charge recommendation. Our present study provides an excellent method for assembling and stabilizing the high-quality organic soluble nanocrystals on large GO sheets. The as-prepared stable GO–TiO_2 NRCs composites can be widely

applied for water purification as well as optoelectronic application at a large scale.

4. Experimental Section

Materials: Sodium nitrate ($NaNO_3$, 99%), potassium permanganate ($KMnO_4$, 99%), hydrogen peroxide (H_2O_2, 35%), concentrated sulfuric acid (H_2SO_4, 98%), oleic acid (OLA, 99%), concentrated hydrochloric acid (36.5%), titanium tetraisopropoxide ($Ti(OPri)_4$ or TTIP, 99%), and trimethylamino-N-oxide dihydrate [$(CH_3)_3NO{\bullet}2H_2O$] were purchased from Sigma-Aldrich (Singapore). Methanol blue was purchased from Reachin Company (Sweden). Natural graphite (SP1) was purchased from Bay Carbon Company (USA). All solvents were purchased from Merck Ltd (Singapore). The DI water was produced by our lab.

Synthesis of Graphene Oxide: The graphene oxide (GO) was synthesized according to the modification of Hummers' methods[29] and the process was described previously.[44]

Synthesis of TiO_2 Nanorods: OLA-capped anatase TiO_2 nanorods were synthesized by hydrolysis of titanium tetraisopropoxide (TTIP) using oleic acid (99%) as surfactant at low temperatures following the modified method published in the literature.[28]

Synthesis of GO–TiO_2 NRCs and GO–P25 Composites: GO (50 mg) and DI water (100 mL) were added into a blue cap bottle (250 mL). The mixture was then sonicated for 1 h to obtain clear solution. TiO_2 nanorods (100 mg) dispersed in toluene (50 mL) was then added into the blue cap bottle. The mixture was kept stirring for 24 h at room temperature to ensure GO coordinated with Ti center on the surface of TiO_2 nanorods. The as-prepared GO–TiO_2 NRCs were purified with large amounts of acetone and centrifuged for 10 min at 10 000 rpm. The obtained GO–TiO_2 NRCs was then washed by THF (100 mL) to get rid of residual oleic acid thoroughly. The final GO–TiO_2 NRCs were then freeze-dried at –50 °C for 48 h. For comparison test, GO (45 mg) and Degussa P25 (100 mg) were added into DI water (200 mL). After the mixtures were sonicated at room temperature for 2 h, the aforementioned mixture were kept stirring for 24 h. The as-prepared GO–P25 composites were centrifuged and free-dried for 24 h for further application.

Characterization: Transmission electron microscopy (TEM) and high-resolution TEM (HRTEM) images were obtained using a JEOL 2010-H microscope (TEM) operating at 200 kV. The samples for the analysis were prepared by dropping dilute toluene solutions of OLA–TiO_2, dilute water solutions of GO and TiO_2 NRCs onto 400-mesh carbon-coated copper grids and leaving the solvent to dry. X-ray powder diffraction (XRD) patterns were taken on a D8-Advance Bruker-AXS diffractometer using Cu Kα irradiation. FTIR spectra were recorded on a Perkin Elmer GX FT-IR system using compressed KBr disc technique. Thermogravimetric analysis (TGA) was performed under dry air using a Perkin Elmer Thermogravimetric Analyzer TGA 7 with Thermal Analysis Controller TAC 7/DX. The samples were heated from room temperature to 900 °C at a rate of 10 °C min^{-1}. XPS measurements were done by using a Kratos Axis Ultra Spectrometer with a monochromic Al Ka source at 1486.7 eV, with a voltage of 15 kV and an emission current of 10 mA. The UV-vis absorption spectra were recorded by using an Evolution 300 spectrophotometer, while photoluminescence (PL) spectra were measured by using a Jobin-Yvon (Fluorolog-3) fluorescence spectrophotometer.

Photocatalytic Experiments: The degradation of MB dyes under UV light irradiation (λ = 254 nm, 11 W, and the light intensity of 5.4 mW cm^{-2}) was observed based on the absorption spectroscopic technique. Typically, aqueous solution of the MB dyes (1 mL, 0.010 mg mL^{-1}) and the photocatalysts (P25/OLA–TiO_2/GO–TiO_2 NRCs/GO–P25 composites, with the same TiO_2 mass of 200 mg) were added into DI water (50 mL) in a cylindrical quartz vessel (150 mL), and the mixture solution was diluted into 100 mL to make sure the MB concentration in the mixture is 10 ppm. For the test of the photocatalytic degradation dynamics of the MB dyes, aqueous solution of the MB dyes (5 mL, 0.010 mg mL^{-1}) and the photocatalysts (73 mg GO–TiO_2 NRCs/GO–P25 composites, with the same TiO_2 mass of 50 mg) were used (the MB concentration in the mixture was 50 ppm). Under ambient conditions and stirring, the photoreaction vessel was exposed to the UV irradiation produced by an 11 W high pressure Hg lamp with the main wave crest at 254 nm and the light intensity of 5.4 mW cm^{-2}. The photocatalytic reaction was started by turning on the Hg lamp, and during the photocatalysis, all other lights were isolated. After given time intervals, the photoreacted solution (5 mL) was analyzed by recording variations of the absorption band maximum (602 nm) in the UV-vis spectra of MB. All the GO–TiO_2 NRCs and GO–P25 photoreacted solutions were centrifuged after adding NaOH (20 mg) to make the desorption of MB from GO. The clear upper solutions were then neutralized with concentrated HCl (0.1 mL, 36.5%) before the UV-vis spectra test.

Supporting Information

Supporting Information is available from the Wiley Online Library or from the author.

Acknowledgements

Authors would like to acknowledge the Clean Energy Research Programme under National Research Foundation of Singapore for their research grant (Grant No. NRF2007EWT-CERP01–0420) support for this work.

Received: July 12, 2010
Published online: September 7, 2010

[1] P. I. Gouma, M. J. Mills, K. H. Sandhage, *J. Am. Ceram. Soc.* **2000**, *83*, 1007–1009.
[2] A. L. Linsebigler, G. Lu, J. T. Yates, *Chem. Rev.* **1995**, *95*, 735–738.
[3] O. Carp, C. L. Huisman, A. Reller, *Prog. Solid State Chem.* **2004**, *32*, 33–177.
[4] H. Yu, X. Quan, S. Chen, H. Zhao, Y. Zhang, *J. Photochem. Photobiol., A* **2008**, *200*, 301–306.
[5] C. He, Y. Xiong, X. Zhu, *Thin Solid Films* **2002**, *422*, 235–238.
[6] V. Subramanian, E. E. Wolf, P. V. Kamat, *J. Am. Chem. Soc.* **2004**, *126*, 4943–4950.
[7] I. Bannat, K. Wessels, T. Oekermann, J. Rathousky, D. Bahnemann, M. Wark, *Chem. Mater.* **2009**, *21*, 1645–1653.
[8] X. Shu, Z. An, L. Wang, J. He, *Chem. Commun.* **2009**, 5901–5903.
[9] T. Tatsuma, S. Saitoh, P. Ngaotrakanwiwat, Y. Ohko, A. Fujishima, *Langmuir* **2002**, *18*, 7777–7779.
[10] Z. Liu, D. D. Sun, P. Guo, J. O. Leckie, *Nano Lett.* **2007**, *7*, 1081–1085.
[11] Y. Yu, J. C. Yu, J. G. Yu, Y. C. Kwok, Y. K. Che, J. C. Zhao, L. Ding, W. K. Ge, P. K. Wong, *Appl. Catal., A* **2005**, *289*, 186–196.
[12] H. Wang, X. Quan, H. Yu, S. Chen, *Carbon* **2008**, *46*, 1126–1132.
[13] X. H. Xia, Z. J. Jia, Y. Yu, Y. Liang, Z. Wang, L. L. Ma, *Carbon* **2007**, *45*, 717–721.
[14] B. Gao, G. Z. Chen, G. Li Puma, *Appl. Catal., B* **2009**, *89*, 503–509.
[15] K. S. Novoselov, A. K. Geim, S. V. Morozov, D. Jiang, Y. Zhang, S. V. Dubonos, I. V. Grigorieva, A. A. Firsov. *Science* **2004**, *306*, 666–669.
[16] D. A. Dikin, S. Stankovich, E. J. Zimney, R. D. Piner, G. H. B. Dommett, G. Evmenenko, S. T. Nguyen, R. S. Ruoff, *Nature* **2007**, *448*, 457–460.
[17] S. J. Park, R. S. Ruoff, *Nat. Nanotechnol.* **2009**, *4*, 217–224.
[18] R. Muszynski, B. Seger, P. V. Kamat, *J. Phys. Chem. C* **2008**, *112*, 5263–5266.

[19] Y. Li, Y. Wu, *J. Am. Chem. Soc.* **2009**, *131*, 5851–5857.
[20] G. M. Scheuermann, L. Rumi, P. Steurer, W. Bannwarth, R. Mulhaupt, *J. Am. Chem. Soc.* **2009**, *131*, 8262–8270.
[21] I. V. Lightcap, T. H. Kosel, P. V. Kamat, *Nano Lett.* **2010**, *10*, 577–583.
[22] G. Williams, B. Seger, P. V. Kamat, *ACS Nano* **2008**, *2*, 1487–1491.
[23] D. Wang, D. Choi, J. Li, Z. Yang, Z. Nie, R. Kou, D. Hu, C. Wang, L. V. Saraf, J. Zhang, I. A. Aksay, J. Liu, *ACS Nano* **2009**, *3*, 907–914.
[24] T. N. Lambert, C. A. Chavez, B. Hernandez-Sanchez, P. Lu, N. S. Bell, A. Ambrosini, T. Friedman, T. J. Boyle, D. R. Wheeler, D. L. Huber, *J. Phys. Chem. C* **2009**, *113*, 19812–19823.
[25] H. Zhang, X. Lv, Y. Li, Y. Wang, J. Li, *ACS Nano* **2010**, *4*, 380–386.
[26] J. Joo, S. G. Kwon, T. Yu, M. Cho, J. Lee, J. Yoon, T. Hyeon, *J. Phys. Chem. B* **2005**, *109*, 15297–15302.
[27] A. Dessombz, D. Chiche, P. Davidson, P. Panine, C. Chanéac, J. P. Jolivet, *J. Am. Chem. Soc.* **2007**, *129*, 5904–5909.
[28] P. D. Cozzoli, A. Kornowski, H. Weller, *J. Am. Chem. Soc.* **2003**, *125*, 14539–14548.
[29] W. S. Hummers, R. E. Offeman, *J. Am. Chem. Soc.* **1958**, *80*, 1339.
[30] P. G. Liu, K. C. Gong, P. Xiao, M. Xiao, *J. Mater. Chem.* **2000**, *10*, 933–935.
[31] Y. W. Jun, M. F. Casula, J. H. Sim, S. Y. Kim, J. Cheon, A. P. Alivisatos, *J. Am. Chem. Soc.* **2003**, *125*, 15981–15985.
[32] C. Xu, X. D. Wu, J. W. Zhu, X. Wang, *Carbon* **2008**, *46*, 386–389.
[33] G. I. Titelman, V. Gelman, S. Bron, R. L. Khalfin, Y. Cohen, H. Bianco-Peled, *Carbon* **2005**, *43*, 641–649.
[34] J. Liu, W. Wang, H. Yu, Z. Wu, J. Peng, Y. Cao, *Sol. Energy Mater. Sol. Cells* **2008**, *92*, 1403–1409.
[35] P. J. Thistlethwaite, M. S. Hook, *Langmuir* **2000**,*16*, 4993–4998.
[36] M. Nara, H. Torii, M. Tasumi, *J. Phys. Chem.* **1996**, *100*, 19812–19817.
[37] D. Gutiérrez-Tauste, X. Domènech, C. Domingo, J. A. Ayllón, *Thin Solid Films* **2008**, *516*, 3831–3835.
[38] T. Szabo, O. Berkesi, P. Forgo, K. Josepovits, Y. Sanakis, D. Petridis, I. Dekany, *Chem. Mater.* **2006**, *18*, 2740–2749.
[39] A. Mills, M. Sheik, C. O'Rourke, M. McFarlane, *Appl. Catal., B* **2009**, *89*, 189–195.
[40] A. Houas, H. Lachheb, M. Ksibi, E. Elaloui, C. Guillard, J. M. Herrmann, *Appl. Catal. B* **2001**, *31*, 145–157.
[41] N. D. Abazović, M. I. Čomor, M. D. Dramićanin, D. J. Jovanović, S. P. Ahrenkiel, J. M. Nedeljković, *J. Phys. Chem. B* **2006**, *110*, 25366–25370.
[42] M. R. Hoffmann, S. T. Martin, W. Y. Choi, D. W. Bahnemann, *Chem. Rev.* **1995**, *95*, 69–96.
[43] C. Y. Kuo, *J. Hazard. Mater.* **2009**, *163*, 239–244.
[44] J. Liu, H. Jeong, J. Liu, K. Lee, J.-Y. Park, Y. H. Ahn, S. Lee, *Carbon* **2010**, *48*, 2282–2289.